Flow analysis of a rotating tidal turbine blade using a dynamic mesh

Vigfús Arnar Jósefsson

FLOW ANALYSIS OF A ROTATING TIDAL TURBINE BLADE USING A DYNAMIC MESH

Vigfús Arnar Jósefsson

30 ECTS thesis submitted in partial fulfillment of a
Magister Scientiarum degree in Mechanical Engineering

Advisor
Halldór Pálsson

Faculty Representative
Sigurður M. Garðarsson

Faculty of Industrial Engineering, Mechanical Engineering and Computer
Science
School of Engineering and Natural Sciences
University of Iceland
Reykjavik, May 2011

Flow analysis of a rotating tidal turbine blade using a dynamic mesh

30 ECTS thesis submitted in partial fulfillment of a M.S. degree in Mechanical Engineering

To my love Heiða Lind and our unborn baby
Thank you for everything

Abstract

The fight against global warming is ongoing, with nations setting forth ambitious goals in reducing greenhouse gas emissions (GHG), both on a national and on a joint international scale. This factor among others is resulting in new power production strategies that focus on renewable energy sources. The ocean is one of those resources with a number of developers trying to develop a technology that will result in the most cost-effective utilization of that resource. Valorka.ehf is an Icelandic company that is developing a new device that utilizes the ocean currents to create power. To support the development of Valorka, a numerical model was built using OpenFOAM. This model consist of a flat plate rotating in a channel, with the model using a dynamic mesh to account for the rotation. This model is supposed to be a startup point of a more complicated model that can be used in the future. The results of the numerical model are compared to measurements that were designed specifically for this project. Also an optimum dimensionless velocity for different blade sizes was found, to confirm if different scales of blade sizes affect the relations found using dimensional analysis. Future work such as blade optimization and 3D modelling is achievable using this model.

Útdráttur

Baráttan gegn gróðurhúsaáhrifunum er í fullum gangi og þjóðir setja sér metnaðarfull markmið í lækkun útblásturs á gróðurhúsalofttegundum. Vegna þessa og annarra áhrifa þá hafa orkuframleiðslustefnur lagt mikla áherslu á notkun endurnýjanlegra orkugjafa. Sjórinn er einn þessara orkugjafa þar sem fjöldi þróunaraðila er að reyna að þróa þá tækni sem mun nýtast best í beislun sjávarorku. Valorka.ehf er íslenskt fyrirtæki sem er að þróa nýjan búnað sem nýtir sjávarstrauma. Til að styðja við þróun Valorku þá var tölulegt líkan smíðað með OpenFOAM hugbúnaðinum. Þetta líkan er af flötu blaði sem snýst í straumi þar sem líkanið notar kvikt net til að herma snúning blaðsins. Þetta líkan er ætlað til að vera upphafstarf að stærra og flóknara líkani sem hægt væri að nota enn frekar við þróun búnaðar Valorku. Niðurstöður frá líkaninu eru bornar saman við mælingar sem hannaðar voru sérstaklega fyrir þetta verkefni. Einnig var fundinn besti einingalausi snúningshraði fyrir mismunandi stærðir blaða til að staðfesta að mismunandi stærðargráður af blöðum sýni sömu tengsl milli víddarlausra stærða sem fundnar voru með víddargreiningu. Hægt er að besta lögun blaðs og smíða þrívítt líkan með notkun þessa líkans.

Contents

Contents

List of Figures

List of Tables

Acknowledgments

This thesis was done under the supervision of Associate Professor Halldór Pálsson at the Faculty of Industrial Engineering, Mechanical Engineering and Computer Science in the School of Engineering and Natural Sciences in University of Iceland. I sincerely thank him for good academic guidance and intellectual support throughout the whole process.

I also thank Valdimar Össurarson, owner of Valorka.ehf, for his time, support and technical assistance in making the experiments a reality. By giving me access to his ideas and work I could also develop the study topics in this thesis.

I would like to express my gratitude to my friend Andri Þór Ingvarsson for giving me access to his video camera.

This project and my M.S. studies were partly sponsored by Landsvirkjun and I thank them dearly for their financial assistance. It was highly appreciated in the final stages of my project work.

Last but not least I would like to thank my family for their encouraging support throughout my education.

1. Introduction

The fight against global warming is ongoing, with nations setting forth ambitious goals in reducing greenhouse gas emissions (GHG), both on a national and on a joint international scale. Another problem is also beginning to affect conventional energy production (i.e. fossil fuelled power plants) which are the ever increasing fossil fuel prices, making that energy source not as cost-effective. The road to a more sustainable development has also been an issue since the publishing of *Our Common Future* (Brundtland et al., 1987), where it is stated that it is fundamental for future generations how the planning and setup of the energy production strategies will be undertaken. The aim for those strategies must be to maximize the sustainability so the footmark on planet earth will not deteriorate the options for the future generations. All of the effects of these issues can be reduced with the use of renewable energy sources.

Using renewable energy sources has gained huge interest the last decade. That interest though has not led to a big jump towards using those renewable sources since other options are still more cost-effective and there are still technological barriers in using them. In USA it is predicted that renewable energy will account for 14% of the total power generation in 2035, only a 3% increase from 2009. This will lead to 0.7% decrease in GHG emissions per capita over the period (EIA, 2011). In Europe the aim is to reach 20% share of renewables in the final energy consumption in 2020, an increase of 9.7% from 2008. Final energy consumption meaning the energy use from all sectors including transport and agriculture (European Union, 2010).

One of the renewable energy sources is the ocean, an energy source that is still not listed as a source when production from renewable energy sources is being compared (European Union, 2010). The main reason behind that is the low accessibility of the resource, needing the use of offshore technology that is still immature and expensive. But this energy source has some benefits. It is often more predictable and its environmental effects are low when compared to other renewable sources, though the environmental effects need more research (Boehlert and Gill, 2010).

There are different harnessable energy forms existing within the ocean. These are the tides (section 2.1) and the ocean currents (section 2.2), wave motion, ocean thermal gradients and salinity gradients. The wave energy resource is estimated to be

1. Introduction

2TW and that estimation is believed to be rather conservative, but only 7-10GW of average power annually seems to be technically available (regardless of cost) (Boyle, 2004). Using the power in the waves to generate electricity got attention in the emerging oil crisis in the 1970's but many countries stopped R&D funding in the 90's (WEC, 2010). Wave power utilization faces difficult challenges such as varying power output, being able to withstand wide range of wave sizes and different incoming wave directions. Ocean Thermal Energy Conversion (OTEC) technology utilizes thermal gradients in the sea. Power can be generated by implementing a Organic Rankine Cycle (ORC) through this temperature difference. The highest gradients exist within the tropics ($\triangle T \sim 20°$) but since this temperature difference is not that high, the maximum theoretical efficency can be expected to be around 7%. Finally there are salinity gradients. These gradients can be used to create power with an osmosis process. Osmotic power plants are still under development, mainly in Netherlands and Norway. Full scale commercialisation is not expected to be achieved until at least in 5 to 10 years (Bedard et al., 2010).

When using the kinetic energy of the ocean and tidal currents, the most popular concept under development is the Horizontal Axis Turbine (HAT). It is a device that has the same working principles as commercial wind turbines (more information is shown in section 2.3). But now a new turbine is being proposed by the company Valorka, a turbine that uses the impulse force of the flowing water to convert the kinetic energy to rotational kinetic energy. This turbine is under development and there are still some important parameters that need to be investigated before a prototype can be built (more information is shown in section 2.4).

The objective of this study is to build a numerical model that can be used to support the development of this new turbine. The numerical model will be validated with measurements that were done in the experimental facilities that are used for the turbine development. The model consists of a rotating flat plate in a flowing fluid with the torque acting on the blade being the main parameter under investigation. This model is then used to find the optimum angular velocity when considering the power output. It is also supposed to be used for future work such as blade optimization and 3D modelling. The model uses a dynamic mesh to account for the blade rotation. Image processing methods are used to analyse the measurements, demonstrating how those methods can be used to gather data instead of using computer connected equipment that logs data directly when measuring the relevant parameters.

The software used to build the model is OpenFOAM. It is an open source software, produced and distributed by OpenCFD® in the UK. It is a multi-discipline solver for differential equations though its main purpose is to be a CFD toolbox. It has gained an interest since it is an open software and has the option for users to develop their own applications or specialized solvers that they can use to solve their problems. The OpenFOAM community is developing additional versions of the original one distributed by OpenCFD®. These versions have extended the tool-

2

box and developed additional applications and solvers. In the study presented in this thesis, one of those versions were used. This version is the OpenFOAM 1.5-dev version that is developed mainly by Prof. Hrvoje Jasak, owner of Wikki (WIKKI, 2011). This version includes tools for implementing and using dynamic mesh, tools that are primarily used in this study.

2. Ocean energy

In this chapter a brief overview is given on ocean current energy in general and how it can be harnessed. A summary of ocean current technology developers is also given, explaining how far each of them has reached in the development stage of their equipment. The last section includes a description of the Valorka turbine, including its design and development status.

2.1. Tides

The gravitational pull of both the sun and the moon on the sea gives rise to periodic movement of the sea towards the attractive potential. The moon's effect on this phenomenon is much bigger than the sun's since it is located much closer to the earth (Boyle, 2004). This is known as the sea tides. Like mentioned earlier, they are periodic in nature and power production from them is highly predictable. This is not common to all renewable energy sources and is considered highly beneficial when considering stability of power production. The technology commonly used to capture this phenomenon is similar to the hydroelectrical concept. A barrage or low dam is built and used to create head when the flood or the ebb tide is occurring. The head (i.e. potential energy) then results in flow (i.e. kinetic energy) where turbines capture it (i.e. rotational kinetic energy) and they turn a generator (i.e. electricity). This renewable energy form is sometimes said to be lunar sourced instead of solar sourced like most other renewable energy sources (e.g. wind-, solar thermal- and photovoltaic energy), since the moon has the biggest influence on it. The energy dissipated from tides globally is estimated to be around 3000 GW and of that amount, only 1000GW are accessible in shallow sea areas. The real potential is much lower and it has been predicted that only 100 GW can be captured, about 15% of the total existing hydroelectric capacity (Boyle, 2004).

2.2. Ocean and Tidal currents

Using the horizontally flowing sea or more specifically the kinetic energy of it directly is an option that has gained interest in recent years. Instead of building costly dams and utilizing the accumulated potential energy (i.e. head) in front of them, the ocean or tidal current is used directly. This energy form is in principle similar to wind energy and devices being developed have many things in common with a wind turbine. Often these turbines are called tidal current turbines but there is some confusion inflicted with that statement. Currents in the sea are caused by two things, first the gravitational pull of the moon and the sun (i.e. tides) and secondly the thermal gradients within it (e.g. Gulf Stream) (Boyle, 2004). So Ocean Current Turbine (OCT) is a more descriptive name on this technology. See section 2.3 for a summary on development of OCT's. This energy form is what the Valorka turbine uses.

2.3. Development of ocean current technology

The ocean current technology did not receive any attention until the 1990's and wave energy and tidal barrages had much more interest by the research community before that. The development of OCT's has gained more momentum in the last two decades. The first devices ready to be tested came to existence around 2000 (WEC, 2010). In (Boyle, 2004) it is predicted that OCT will overtake wave energy and mature sooner since the industry can learn a lot from wind energy technologies and its environment is more predictable.

When making comparison between ocean current energy and wind energy some care must be taken. Although the two resources are similar in nature where a mass of flowing fluid is the energy source, there are some differences. The sea is much denser than air so with a fluid moving at the same velocity the energy density is roughly 1000 times higher. Also, the wind is only constrained by the lower surface when flowing through wind turbines while the sea is bounded by the ocean floor and the free surface above and sometimes also by the geological settings in the ocean (e.g. narrow flow channels) (Robinson and Byrne, 2008). Other differences can be mentioned such as the Reynolds number of the flow, occurence of cavitation and wave motion (Turner and Owen, 2007).

The development community mainly consists of many small developers backed by government funding and only small portion of these developers are testing full scale prototypes (Bedard et al., 2010). In the following subsections a list of some of the developers in alphabetical order that are considered most promising in this field (Rourke et al., 2010).

2.3.1. DeltaStream Turbine

This device has 1.2 MW power output. It consists of three turbines mounted on the same 30 m wide triangular frame that is fixed to the seafloor. The three turbines are horizontal axis turbines, having the same working principles as wind turbines supported by ship propeller technology. The frame gives the device a low center of gravity and enhanced stability (Tidal Energy Ltd., 2011). On the 31st. March 2011 Tidal Energy Ltd. got allowance for assembling and testing the DeltaStream turbine in West Wales. It will be grid connected and operate at 1.2 MW during the test period for 12 months (DECC, 2011).

2.3.2. Evopod Tidal Turbine

Ocean Flow Energy Ltd. developed the Evopod. This turbine is a five-blade horizontal axis turbine (HAT) that uses a lot off-the-shelf equipment from shipping and wind power industries. Its main distinction is that it is a floating device that is moored to the seafloor and it always keeps optimum heading into the current. It can be accessed by ship for first line maintenance. A 1/10th scale model has been tested during 2008 and 2009 in Strangford Narrows, Northern Ireland. The testing proved successful. Last year was used to extend the installation to electrical grid connection. A scaled up version of the 1/10th scale model (Power output 35-55kW) is under development and will be available as grid connected or off-grid device (Ocean Flow Energy Ltd., 2011).

2.3.3. Free Flow Turbine

This turbine as seen in figure 2.1 was installed 2008 in NYC East River and has produced 70MWh of energy to NYC customers and operated for 9000 turbine hours. It is a three bladed HAT that was developed by Verdant Power. It consisted of a rotor 5 m in diameter and yawing mechanism to operate both on the ebb and the tide. During the test period five turbines were connected in array, making it the first electrical grid connected ocean current turbine (OCT) array. During the next years the plan is to install a 1 MW, 30 OCT array in the East River and deliver commercially electricity to NYC customers (Verdant Power Inc., 2011).

Figure 2.1: The Free Flow Turbine. Credit: Verdant Power, Inc.

2.3.4. Lunar Energy Tidal Turbine

This turbine is also a HAT (see Figure 2.2), just as the Free Flow turbine. It has a duct that is used instead of a yawing mechanism to capture incoming flow not parallel to the turbine's axis. Ducting increases the theoretical maximum efficiency of the turbine since it captures incoming flow larger in diameter than a bare rotor with no ducting. Also flow speed can be enhanced by using the hydrostatic pressure in the ocean (i.e. diffusing). A gain of 100% in potential power output has been reported for ducted OCT's (Robinson and Byrne, 2008). Lunar Energy Ltd. agreed to a £500 million deal to install 300 OCT's off the coast of Korea in 2008. This device is still under development and it looks like nothing has been built yet (Lunar Energy Ltd., 2011).

2.3.5. Atlantis Resources Corporation Turbines

The Atlantis Resources Corporation is developing three turbines, the AK, AS and AN series. The AK series is a twin rotor HAT with power output of 1MW. It is the newest turbine of the three. It has been in testing at EMEC and its blades are being replaced (early 2011) after its old blades failed and broke during testing. Each rotor operates only on the flood or the tide.
The AS series is a ducted HAT and was tested in 2008. It is available in 100 kW,
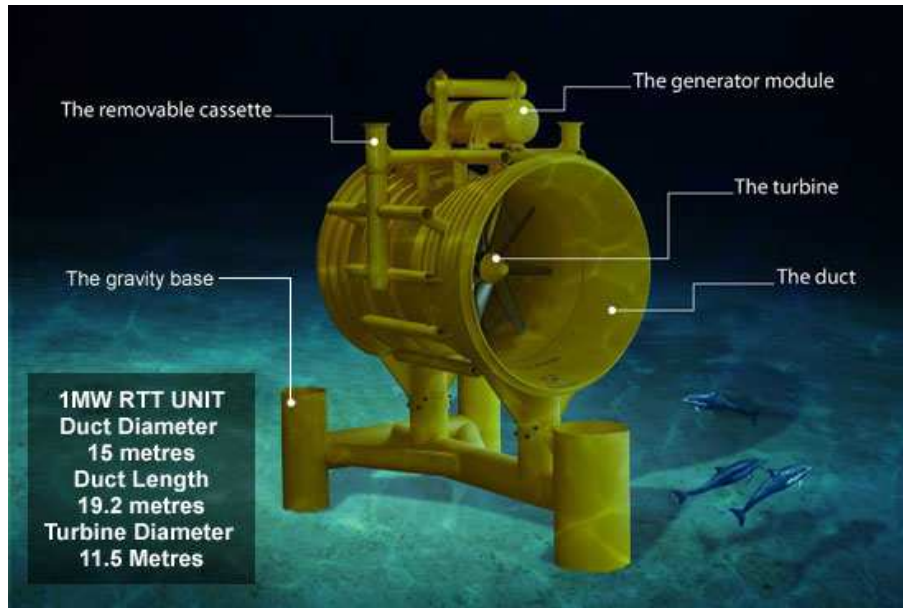
Figure 2.2: The Lunar Energy Turbine. Credit: Lunar Energy Ltd.

500 kW or 1 MW configurations. It is recognized as the most efficient water-to-wire turbine in the world.

Finally there is the AN series. This turbine uses Aquafoils™ to capture momentum to drive a chain perpendicular to the flow. This is a shallow water model designed to withstand a flow with significant amount of debris. Testing has been done in 2008 and it has been developed over a 6 year period. Atlantis Resources Corporation currently seems to focus most on the new AK series and its testing at EMEC (ARC, 2011).

2.3.6. Open-Centre Turbine

This turbine was the first one to be tested at EMEC, in the beginning of 2006. It is a simple design and the test unit of 6m diameter in size produced enough electricity for 150 average european homes. It is a ducted horizontal axis turbine with the generator included in the same module as the rotor/stator and the duct. OpenHydro has announced two big projects in Nova Scotia Canada and in the Channel Islands just outside the coast of France, where the plan is to build tidal farms in the future. When being tested at EMEC it was the first OCT to be connected to UK national electricity grid (OpenHydro, 2011).

2.3.7. Pulse Tidal Hydrofoil

Pulse Generation Ltd. developed this device. This device is considered to be non-conventional since it is not a rotating turbine. It consists of large hydrofoils that move up and down and can be used in shallow waters since it does not require the same depth as a large rotor. The developer states that operation and maintenance (O&M) of this device is less of a problem compared to other devices installed at deeper sea levels. A 100kW unit has been producing electricity in the mouth of River Humber in the UK from 2009 (Pulse Generation Ltd., 2011). Also an agreement has been reached that the company will install a 1.2MW single device in the Isle of Skye waters in Scotland in 2012 and produce electricity. If successful, eight devices could be stringed together to produce 9.6MW of power (BBC, 2011).

2.3.8. SeaGen

The first commercially available turbine is developed by Marine Current Turbines (MCT) Ltd. It is now operating at 1.2MW (full power) in Strangford Narrows, Northern Ireland, and is able to produce of 10 MWh of energy per tide, adding up to 6000 MWh per year. This amount is similar to what a wind turbine of 2.4 MW produces in one year. MCT states that this shows that ocean currents are not only more predictable but also twice as productive than wind. This device is a twin rotor HAT device where each rotor is 16m in diameter. Both rotors work on the flood and the ebb and it rotates its pitch angles through 180° to be able to do so. The rotors are mounted on a steel monopile that can be raised out of the water for easier maintenance (MCT, 2011).

2.3.9. Tidal Stream Turbine

The first OCT to be connected to a electrical grid ever, back in 2003, was the HS300. It is a 300 kW prototype that was installed in Kvalsund, Norway, developed by Hammerfest Strom AS. Its design is mainly built on wind turbine design principles and therefore is a three bladed HAT machine. Now the company is developing a scaled up version of the HS300, called HS1000. The plan is to test that machine at EMEC during the summer of 2011. It is rated at 1 MW power output for current velocities of 2.5 m/s (Hammerfest Strom AS, 2011).

2.4. The Valorka turbine

All of the devices in section 2.3 are mainly using the lift force created when flow velocities around the turbine blade are not the same, resulting in a pressure difference across the blade. Such setups are commonly known as reaction turbines. Also, they are designed for current velocities around 2.5 m/s and their design is using a lot of off-the-shelf equipment from the wind turbine and shipping industry. In contrast, the Valorka turbine uses mainly the impulse force created when the flow hits the turbine blade and it is designed for low speed currents (less than 2.5 m/s). Its design is based on the old water wheel concept that was first used centuries ago. The water wheel operates partially submerged in water, using the drag force created by the water jet impinging on it. The Valorka turbine operates basically in the same way but it is fully submerged and it uses some novel methods to be able to function that way.

The 4th. edition of its design is being developed right now (May 2011) and testing is being done on a small scale model. Next phase of the development includes upscaling the model and sea testing. The Valorka Turbine project has got R&D funding from Rannis Technology Development Fund and the Energy Fund from National Energy Agency and currently more funding is being requested. This project started in 2008 and has been ongoing since (Valorka, 2011).

Figure 2.3: Small scale model of the 4th. edition of the Valorka Turbine.

The current edition being developed now is a crossflow device (i.e. axis perpendicular and horizontal to the flow) that has a multiple pairs of blades that rotate about a

common axis. Each blade is on its own shaft and it can rotate 90°. When in the right position the surface of the blade will be perpendicular to the flow and after the turbine has rotated half a circle, the same blade will close (i.e. blade parallel to the flow) to minimize the impulse force on the way back to opening position. This model rotates in the same direction for both flow directions. The blade opens up either in the lower half of the rotational cycle or the upper half, depending on the rotational and flow directions. Figure 2.3 is an image of a small scale model that was used in tests. (Valorka.ehf, 2010).

3. Theory

The well known Navier-Stokes equations are the governing equations for this fluid flow problem. The flow in this study is assumed to be incompressible and with constant fluid properties. The flow is also considered to be in the turbulent regime. A discussion on how turbulence is added to the governing equations is also included in this section. Using a dynamic mesh introduces a new term in the governing equations that will be showed here along with the method that is used to transmit flow variables across the rotational and stationary interface.

3.1. Navier-Stokes equations

The continuity equation for incompressible flow can be expressed in general form as

$$\nabla \cdot \mathbf{v} = 0 \tag{3.1}$$

since density of the fluid is constant. Here, $\mathbf{v}$ is the velocity vector.

The momentum equation for incompressible flow in general form can similarly be written as

$$\frac{\partial \mathbf{v}}{\partial t} + (\mathbf{v} \cdot \nabla)\mathbf{v} = -\frac{1}{\rho}\nabla p + \nu \nabla^2 \mathbf{v} + F \tag{3.2}$$

where ρ is the fluid density, p is the pressure, ν is the kinematic viscosity and F represents body forces. For more information on the derivation of these equations refer to (Rutherford, 1989).

Since the model developed in this study is a 2D model, the governing equations are written in Cartesian form for two coordinates as following, beginning with eq. 3.1

$$\frac{\partial u}{\partial x} + \frac{\partial v}{\partial y} = 0 \tag{3.3}$$

where u is the flow velocity in the x-direction and v is the flow velocity in the y-direction.

Doing the same for eq. 3.2 and writing out the equation explicitly for each coordinate direction leads to

$$\frac{\partial u}{\partial t} + \left(u\frac{\partial u}{\partial x} + v\frac{\partial u}{\partial y}\right) = -\frac{1}{\rho}\frac{\partial p}{\partial x} + \nu\left(\frac{\partial^2 u}{\partial x^2} + \frac{\partial^2 u}{\partial y^2}\right) + F_x \tag{3.4}$$

$$\frac{\partial v}{\partial t}+\left(u\frac{\partial v}{\partial x}+v\frac{\partial v}{\partial y}\right)=-\frac{1}{\rho}\frac{\partial p}{\partial y}+\nu\left(\frac{\partial^2 v}{\partial x^2}+\frac{\partial^2 v}{\partial y^2}\right)+F_y \tag{3.5}$$

where F_x and F_y represent body forces in each direction.

3.2. Reynolds Averaged Navier-Stokes modelling

When the flow becomes unstable, the flow is said to be turbulent. The length and time scales in turbulence are much smaller than the physical length and time scales for the flow problem and are very CPU expensive to simulate in detail. Reynolds Averaged Navier-Stokes (RANS) modelling is an approximation to real turbulence where the velocity fluctuations are represented by one mean component and another fluctuating component. If velocity is taken as the flow variable, it is decomposed to

$$u(x,t)=\overline{u}+u' \tag{3.6}$$

where u' is the fluctuating component and $\overline{u}$ is the mean component. The mean component is defined as for unsteady flows

$$\overline{u}=\lim_{T\to\infty}\frac{1}{N}\sum_{n=1}^{N}u(x,t) \tag{3.7}$$

which is called ensemble averaging where N is the number of members in the ensemble. N has to be large enough so that the influence of the fluctuations are not seen when calculating eq. 3.7. For more information about ensemble averaging refer to (Ferziger and Peric, 2002).

Averaging the linear terms in eq. 3.3, eq. 3.4 and eq. 3.5 will just give the same terms but now for the mean component. But when the nonlinear terms are averaged two terms are found instead of one, product of the mean components term and a covariance term. More specifically

$$\overline{uv}=\overline{(\overline{u}+u')(\overline{v}+v')}=\overline{u}\,\overline{v}+\overline{\overline{u}v'}+\overline{\overline{v}u'}+\overline{u'v'}=\overline{u}\,\overline{v}+\overline{u'v'} \tag{3.8}$$

since the average of a fluctuation is zero. The last term is the *covariance*.

Now eq. 3.3, eq. 3.4 and eq. 3.5 can be written for turbulent flow using the aforementioned approximation. Continuity equation eq. 3.1 has the same form as before

$$\nabla\cdot\overline{\mathbf{v}}=0 \tag{3.9}$$

Now the momentum equation eq. 3.2 becomes as follows when introducing the new terms

$$\frac{\partial\overline{\mathbf{v}}}{\partial t}+\left(\overline{\mathbf{v}}\cdot\nabla\right)\overline{\mathbf{v}}=-\frac{1}{\rho}\overline{\nabla p}+\nu\nabla^2\overline{\mathbf{v}}-\nabla\cdot\overline{\boldsymbol{\tau}}_{ij}+F \tag{3.10}$$

where $\overline{\boldsymbol{\tau}}_{ij}$ is the *Reynolds Stress tensor* defined as

$$\overline{\boldsymbol{\tau}}_{ij} = \overline{v_i' v_j'} \tag{3.11}$$

with i and j denoting individiual tensor components.

This additional term makes the Navier-Stokes equations not a closed set of equations or simply it has more unknowns than equations. New relations are needed to make up for that and that is the purpose of using turbulence models (Ferziger and Peric, 2002)(Tennekes and Lumley, 1974).

3.3. k−ϵ turbulence model

The most common and well known turbulence model is the standard $k - \epsilon$ model (Ferziger and Peric, 2002). It is a high Reynolds number eddy-viscosity model that is derived using the Boussinesq assumption. It relates the *Reynolds stresses* to a turbulent viscosity μ_t multiplied with the velocity gradients. Or in more detail (using index notation)

$$-\rho \overline{u_i' u_j'} = \mu_t \left(\frac{\partial \overline{u}_i}{\partial u_j} + \frac{\partial \overline{u}_j}{\partial u_i} \right) - \frac{2}{3} \delta_{ij} \rho k \tag{3.12}$$

where the last term is needed to make the equation hold when it is contracted (indices set equal and summed over). In eq. 3.12, k is the turbulent kinetic energy

$$k = \frac{1}{2} \overline{u_i' u_i'} \tag{3.13}$$

Turbulence is described by a mininum of two quantities, a velocity scale and a length scale. Models that use two transport equations to find these quantities are known as two equations models. The $k - \epsilon$ model is one of those models, using the turbulent kinetic energy k and the dissipation ϵ to describe them. The exact equation for k is derived from the Navier-Stokes equations and is expressed as for incompressible and constant viscosity flow

$$\frac{\partial(\rho k)}{\partial t} + \frac{\partial(\rho \overline{u}_j k)}{\partial x_j} =$$
$$\frac{\partial}{\partial x_j} \left(\mu \frac{\partial k}{\partial x_j} \right) - \frac{\partial}{\partial x_j} \left(\frac{\rho}{2} \overline{u_j' u_i' u_i'} + \overline{p' u_j'} \right) - \rho \overline{u_i' u_j'} \frac{\partial \overline{u}_i}{\partial x_j} - \mu \overline{\frac{\partial u_i'}{\partial x_k} \frac{\partial u_i'}{\partial x_k}} \tag{3.14}$$

Different terms in eq. 3.14 have different physical meaning. The two terms on the left hand side represent transient changes and convection respectively. The first term on the right hand side denotes *viscous diffusion* and the next two terms denote

the *turbulent diffusion* by pressure and velocity fluctuations. This therm is modeled by gradient diffusion assumption

$$\left(\frac{\rho}{2}\overline{u_j' u_i' u_i'} + \overline{p' u_j'}\right) \approx \frac{\mu_t}{\sigma_k}\frac{\partial k}{\partial x_j} \tag{3.15}$$

where the eddy viscosity is $\mu_t = C_\mu \rho q L$, with C_μ as a dimensionless constant, q as a velocity scale and L as a length scale. σ_k is a *turbulent Prandtl number* that is close to unity.

The fourth term in eq. 3.14 is the *rate of production* of turbulent kinetic energy using energy extracted from the mean flow. If eq. 3.12 is used to represent the *Reynolds Stress*, this term can be modeled as

$$P_k = \rho \overline{u_i' u_j'}\frac{\partial \overline{u}_i}{\partial x_j} \approx \mu_t \left(\frac{\partial \overline{u}_i}{\partial u_j} + \frac{\partial \overline{u}_j}{\partial u_i}\right)\frac{\partial \overline{u}_i}{\partial x_j} \tag{3.16}$$

The last term in eq. 3.14 is the *dissipation* of small scale kinetic energy to internal energy. The dissipation is

$$\epsilon = \nu \overline{\frac{\partial u_i}{\partial x_j}\frac{\partial u_i}{\partial x_j}} \approx \frac{k^{\frac{3}{2}}}{L} \tag{3.17}$$

The modelled equation for the *dissipation* is as following in its most common form

$$\frac{\partial(\rho\epsilon)}{\partial t} + \frac{\partial(\rho u_j \epsilon)}{\partial x_j} = C_{\epsilon 1}P_k\frac{\epsilon}{k} - \rho C_{\epsilon 2}\frac{\epsilon^2}{k} + \frac{\partial}{\partial x_j}\left(\frac{\mu_t}{\sigma_\epsilon}\frac{\partial \epsilon}{\partial x_j}\right) \tag{3.18}$$

The model discussed here is the $k - \epsilon$ model based on the two equations, eq. 3.14 and eq. 3.18 (Davidson, 2011). The five unknown constants in the model are usually given the following values (Ferziger and Peric, 2002):

$$C_\mu = 0.09 \quad C_{\epsilon 1} = 1.44 \quad C_{epsilon2} = 1.92 \quad \sigma_k = 1.0 \quad \sigma_\epsilon = 1.3 \tag{3.19}$$

3.4. Navier-Stokes for a dynamic mesh

A dynamic mesh is ideal for use in rotor-stator turbomachinery simulations. The Navier-Stokes equations for an incompressible fluid are defined as follows in arbitrary Lagrangian-Eulerian formulation for a dynamic mesh. Now written in integral form for a control volume, the continuity equation is as follows

$$\frac{\partial}{\partial t}\int_V dV + \int_S (\mathbf{v} - \mathbf{v_b}) \cdot \mathbf{n}\, dS = 0 \tag{3.20}$$

And the momentum equation is expressed as

$$\frac{\partial}{\partial t}\int_V \rho \mathbf{v} dV + \int_S (\rho \mathbf{v}(\mathbf{v} - \mathbf{v_b}) + p\mathbf{I} - \boldsymbol{\tau}) \cdot \mathbf{n}\, dS = 0 \tag{3.21}$$

where $\mathbf{v_b}$ is the boundary (S) velocity of the control volume (V), $\mathbf{v}$ is the fluid velocity in fixed coordinate system, p is the pressure, $\mathbf{I}$ is the unit tensor, τ is the viscous stress tensor and $\mathbf{n}$ is the outward normal. The viscous stress tensor is defined as before for incompressible Newtonian fluid

$$\boldsymbol{\tau} = \mu \left(\frac{\partial v_i}{\partial x_j} + \frac{\partial v_j}{\partial x_i} \right) \tag{3.22}$$

where μ is the dynamic viscosity (Riemslagh et al., 1998).

The velocity $\mathbf{v_b}$ has to satisfy a space conservation law additionally since conservation is not ensured when the mesh velocities are used to calculate the mass fluxes (e.g. mass conservation). For detailed discussion see (Ferziger and Peric, 2002). This space conservation law is expressed as

$$\frac{\partial}{\partial t} \int_V dV - \int_S \mathbf{v_b} \cdot \mathbf{n} dS = 0 \tag{3.23}$$

3.5. General Grid Interface

General Grid Interface (GGI) is an interface developed to couple non-conformal meshes together. When there are complex geometries or moving meshes it is often convenient to develop the mesh by creating number of meshes that represent different regions in the solution domain. Usually it is very hard to let these meshes to be conformally joined (i.e. each node on either side of the coupling interface are matched one to one). These meshes can then be coupled by using one or more GGI's.

The GGI uses weighted interpolation to calculate and submit flow variables across the interface. It can be thought of as "static" sliding interface that does not need to re-mesh the cells close to the interface. If a master patch and a shadow patch are defined as the patches on each side of the interface, the flow values from one patch to another are defined as

$$\phi_{Si} = \sum_n W_{M_n-to-S_i} * \phi M_n \qquad \phi_{Mj} = \sum_m W_{S_m-to-M_j} * \phi S_m \tag{3.24}$$

where M_j denotes the jth master face, S_i the ith shadow face, n and m are the number of master and slave faces neighbours for either M_j or S_i and W is the weighting factor for both sides. For the weighting factor to remain conservative its sum from eq. 3.24 is equal to unity.

The value of the weighting factors can be found with

$$W_{M-to-S_i} = \frac{|\underline{S}_{\cap M-to-S_i}|}{|\underline{S}_{M_n}|} \qquad W_{S-to-M_j} = \frac{|\underline{S}_{\cap S-to-M_j}|}{|\underline{S}_{S_m}|} \tag{3.25}$$

where $|\underline{S}_{\cap M-to-S_i}|$ and $|\underline{S}_{\cap S-to-M_j}|$ are the surface intersection area between master and shadow patch faces, and $|\underline{S}_M|$ and $|\underline{S}_S|$ are the surface areas of a master and

shadow patch faces. The evaluation of the intersection surface area is done by using the 2D face-to-face intersection Sutherland-Hodgman algorithm (Sutherland and Hodgman, 1974). It is very generic and is very easy and compact for source code implementation. To determine the neighbourhood of cells related to the face being evaluated, an optimized search and quick-reject tests are used. For more detailed discussion on GGI, refer to (Beaudoin and Jasak, 2008)

3.6. Average torque calculation

The torque acting on the blade is a function of time. The torque appears because of drag and viscous forces (mainly drag) acting on the blade due to fluid flow past it. The most important parameter in this study is the average torque acting on the blade during its rotation. The reason for that is because the objective is to maximize it since it gives the highest average power output. To find this parameter, the torque needs to be integrated over the time interval and then divided by the same time interval to reach the average torque. This is expressed mathematically in the following way

$$\overline{T}_{ave} = \frac{1}{\tau} \int_{t_0}^{\tau} T dt \tag{3.26}$$

where τ is the time interval and t_0 denotes the starting time.
This integration has to be done numerically and it was done using the trapezoidal rule

$$\overline{T}_{ave} = \frac{1}{\sum_{i=2}^{n}(t_i - t_{i-1})} \sum_{i=2}^{n}(t_i - t_{i-1})\left(\frac{T_{i-1} + T_i}{2}\right) \tag{3.27}$$

where t_i and T_i are the time and torque outputs with i denoting the number of outputs.

4. Case Study

Some aspects of the development of the numerical model will be mentioned here such as building the mesh, which boundary conditions were used and how the original code was edited to be able to do time dependent blade rotation. Also the experimental setup and how the data was analysed will be described.

4.1. Numerical model

This section covers the setup of the numerical model and the measurement procedure. The process of setting up the numerical model is explained and some discussion given on what methods are used to solve the problem. The experimental setup is then described along with a introduction to the image processing used to analyse the measured data.

4.1.1. Geometry and mesh

The geometry and the mesh were built using the *blockMesh* utility that is distributed with the OpenFOAM package. This utility has no Graphical User Interface (GUI) and all the setup is done via a text file. This utility is convenient to use when building simple geometries. The domain is built of hexahedral blocks that can have curved edges and they can be graded, so they need not to be uniformly distributed in one direction. The hexahedral blocks make the mesh three dimensional but special boundary conditions for the cell faces in the third dimension are used so the model is a true 2D model (see sec. 4.1.3). Figure 4.1 shows the overall solution domain. The top and bottom boundaries are 5 blade lengths above and below the blade itself. This length was considered enough so it would not affect the flow over the blade. And the inlet and outlet boundaries are 8 blade lengths away from the center point for the same reason.

The circumferential interface that can be seen clearly in fig. 4.2 is the interface where the rotational and stationary parts of the mesh meet. This interface uses a weighted interpolation (see sec. 3.5) to transmit flow variables accross it.
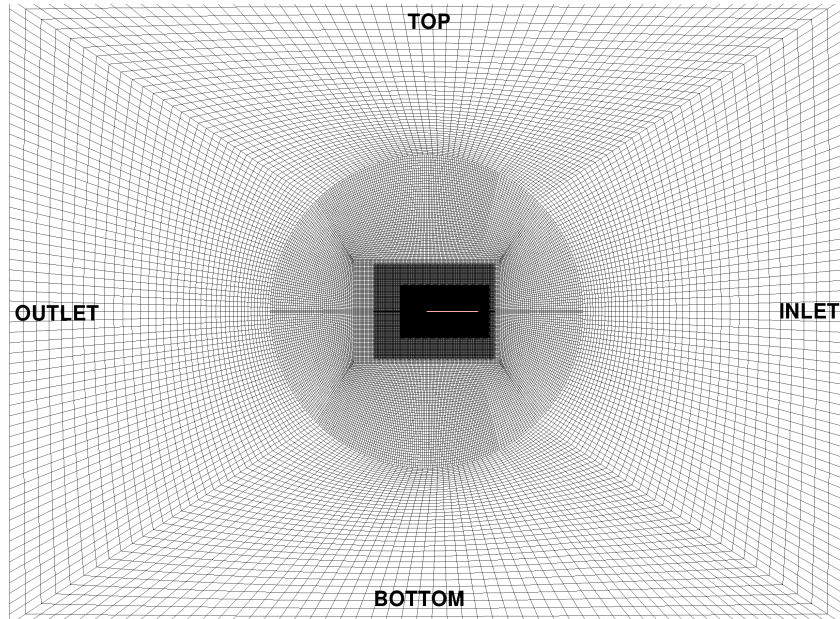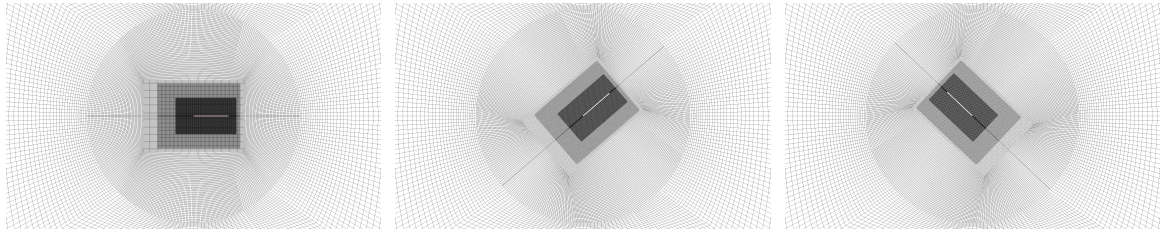
Figure 4.1: The solution domain.

Figure 4.2: The rotation of the mesh

The area around the blade was refined specially with the *refineMesh* utility that is a part of the OpenFOAM package. This utility splits one cell into four cells, with new cell faces having half of the length of the cell face length of the original cell. The blade itself is a smooth rectangular flat plate with sharp corners. The blade with some refined cells can be seen in fig. 4.3.

4.1.2. Time dependent blade rotation

The standard class *mixerGGIFvMesh* in OpenFOAM 1.5-dev is only able to handle constant angular velocity. It is needed to make the angular velocity as a function of time so the simulations can be compared to various real cases. This modification is rather easy and only a basic understanding of a C++ code is needed.

The rotation was hardcoded into the code using *if* sentences. The angular velocity is defined in rounds per minutes (rpm) in the code and the mesh points are moved by
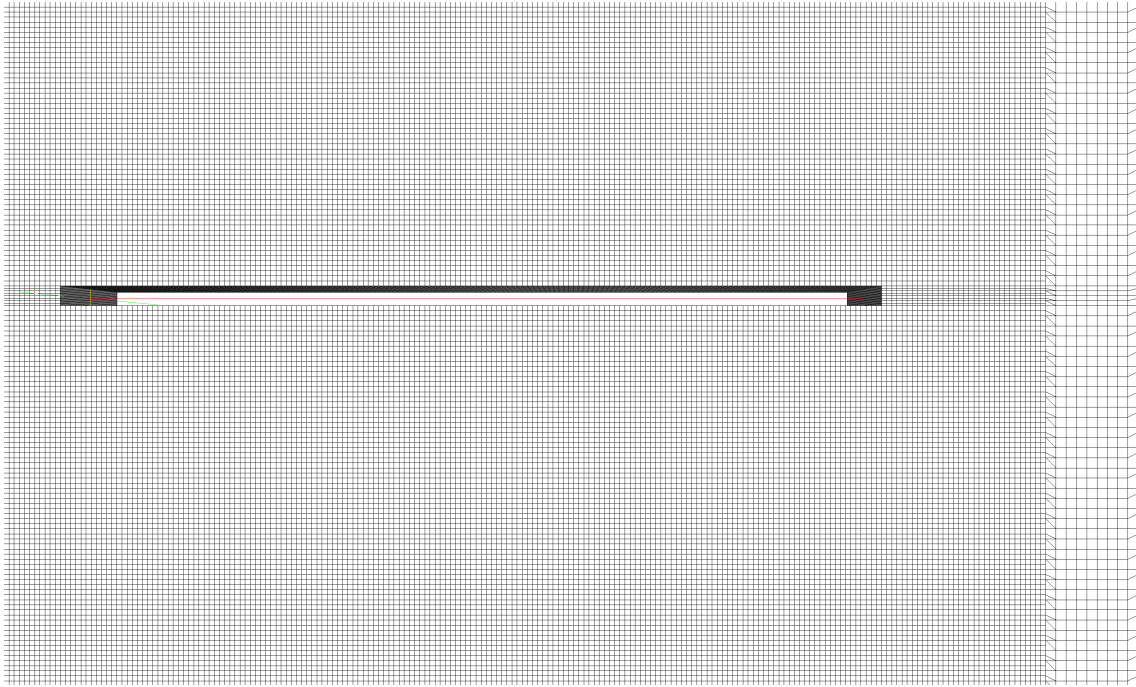
Figure 4.3: The blade with refined cells.

adding a vector to the existing position of the points. The class *mymixerGgiFvMesh* was developed and compiled and added to the OpenFOAM library. The portion of the class that handles the time dependent rotation can be seen below in figure 4.4. The rpm value is now hardcoded into the class and the class uses the current time value to switch between different values of it.

```
bool Foam::mymixerGgiFvMesh::update()
{
 //Logical sentence added by thesis author to control rpm value
 if (time().value() > 0.5)
  {
   rpm_ = 0;
  }

// Rotational speed needs to be converted from rpm (Original code)
   movePoints
   (
     csPtr_->globalPosition
     (
       csPtr_->localPosition(allPoints())
      + vector(0, rpm_*360.0*time().deltaT().value()/60.0, 0)
       *movingPointsMask()
     )
   );

   // The mesh is not morphing
   return false;
```

Figure 4.4: The modified OpenFOAM class.

4.1.3. Boundary conditions

The inflow boundary condition is specified by assigning a constant velocity value at the inlet boundary. The outlet condition is defined as a pressure outlet where a zero gauge pressure is set. The top and bottom surfaces have a "slip" condition assuming non-viscous surfaces. The boundary of the blade has a "no-slip" condition where $u_i = 0$, assuming a viscous fluid with a shear force. This condition is the physically correct one. Wall functions were used to capture the turbulent velocity profile in vicinity of the blade. The inflow conditions of the turbulent kinetic energy and dissipation were assigned a low value on the scale of 10^{-4} since no prior knowledge was attainable for these values. Figure 4.5 shows what boundary conditions were used and where they were added in the solution domain.
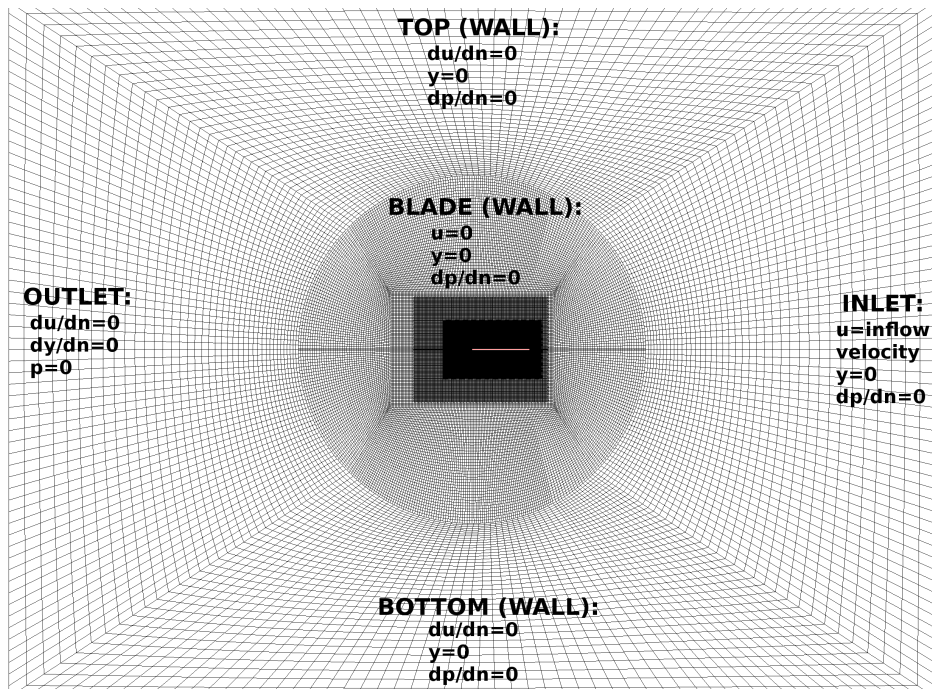

Figure 4.5: Boundary conditions used for the numerical model.

4.1.4. Running the case

The *turbDyMFoam* solver was used to solve the problem. This solver is intented for transient, incompressible, turbulent flows for Newtonian fluids using a dynamic mesh. It uses the SIMPLE and PISO algorithms (Audi, 2009) coupled together to allow for higher Courant number and therefore a longer time step than when only the PISO algorithm is used (Otic and Cheng, 2010).

The simulations that were done for this study were performed in parallel. The computer cluster SOL owned by University of Iceland was used for the computations. The dynamic mesh and GGI are capable of parallelisation. A method was used to decompose the solution domain, that cuts the geometry into equal parts that are specified beforehand. For example when running on four processors with a 2D problem with N^2 nodes (N nodes in each coordinate direction) it is logical to cut the domain in two parts in each direction. In table 4.1 the CPU time is shown for the same case solved by different amount of processors. In figure 4.6 it can be

Table 4.1: CPU time for the same case solved by different amount of processors.

No. processors	CPU time (mins)	Relative CPU speed increase
1	619	1
2	333	1.86
4	219	2.83
8	129	4.80

seen that there is not a pure linear decrease with the amount of processors. This is normal since the time that goes in communication between processors has a higher influence when the number of processors is increased. But this shows clearly the advantage of parallel computing and how it can save time.
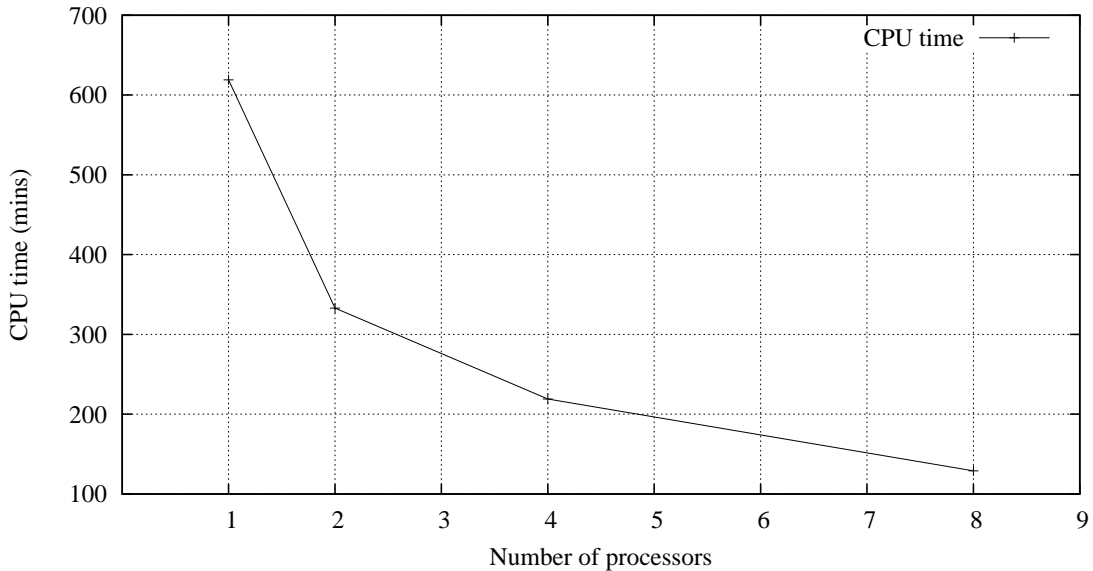

Figure 4.6: CPU time for increasing amount of processors.

4.2. Physical Experiments

The measurements were done in testing facilities that Valorka uses. They have a water tank that allows flow velocity up to $0.45\,m/s$. The measurements were done with video camera and image processing techniques. Since the digital scales used in the experiments did not have high enough response time, some editing of the original setup of the experiments had to be done. Instead of investigating the torque during the 180° rotation which would be optimal, the blade was fixed at certain angles and the torque acting on the blade in that current position measured. This was done for several angles during the 180° rotation.

4.2.1. Experimental setup

The blade used for measurements was 25 cm long and 60 cm wide. It was made out of plexiglass and was flat with rectangular corners. Two aluminium beams were put behind it to enhance structural stability when under loading. Figure 4.7 shows the blade fixed on a frame.
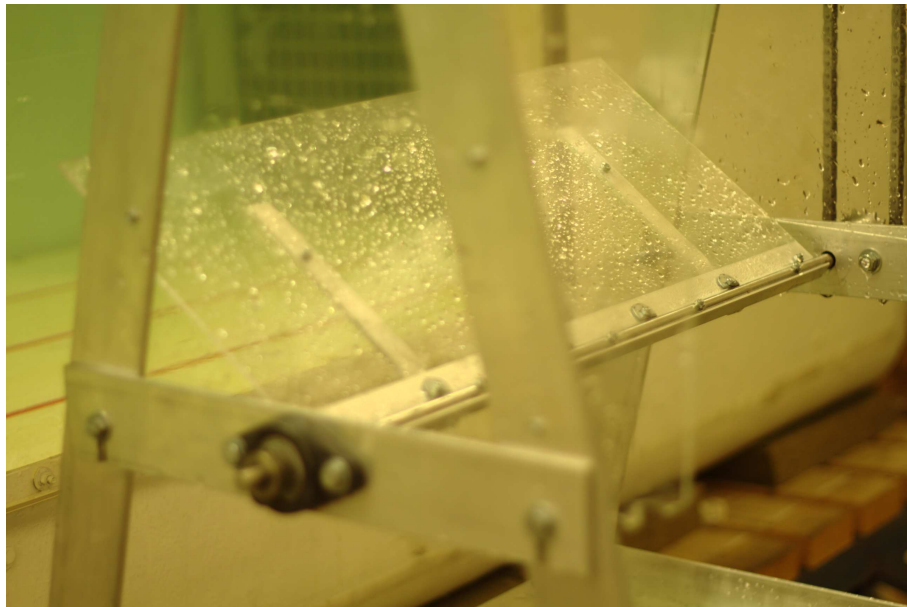

Figure 4.7: The blade used in the experiments.

The shaft connected to the blade turned a wheel that was coupled to another weel on the upper shaft of the frame (figure 4.8). The upper shaft in the frame turned in an equal ratio to the blade shaft. On the opposite end to the one shown in figure 4.8 there was another wheel on the upper shaft. This wheel applied torque on the digital scales and it was 10cm in diameter. The measured weight difference between the

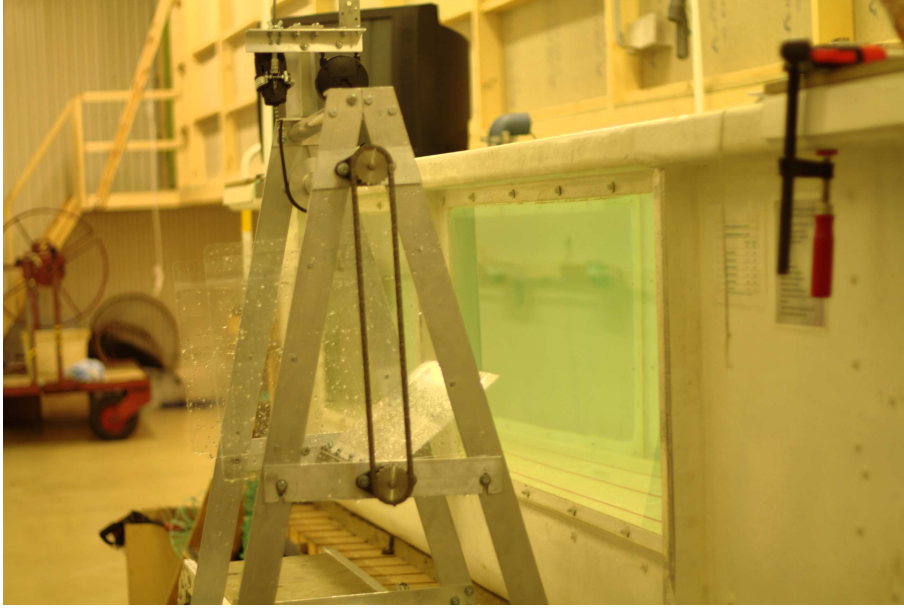scales represented then the torque applied by the blade. The steel frame holding

Figure 4.8: The coupling of the wheels connected to the shafts.

the measurement equipment when in the tank can be seen in figure 4.9. There were two plexiglass sides added close to each end of the blade to minimize side effects in the flow over the blade. These blades were parallel to the flow and they acted as a blockage on the flow when it would flow over the blade sides. The blade was fixed by increasing the weight load (i.e. resistance) on the scales until it was large enough to hold the blade in place. The measurements were done with flow velocity of (0.4 ± 0.03)m/s and the torque was measured for five different blade angles. The blade angle was roughly set and it was found afterwards in the postprocessing, using the methods described in 4.2.2. Figure 4.10 shows the blade in a fixed position when the torque was being measured.

4.2.2. Data analysis with image processing

The videos captured in the measurement process were broken down frame by frame and imported as images into MATLAB. There it is possible to use the Image Processing Toolbox to manipulate the images and capture relevant features from them. The most important thing was to be able to determine the angle of the blade. This was done by using a red colored pencil as a pointer that rotated in a 1:1 ratio with the blade itself. Fig. A.3 shows three different unprocessed frames from one of the videos. By letting MATLAB analyse the video frame by frame, the red pencil could be isolated easily since its red component in the RGB value is higher than for other colors in the images. Then by switching off all pixels except those that have high
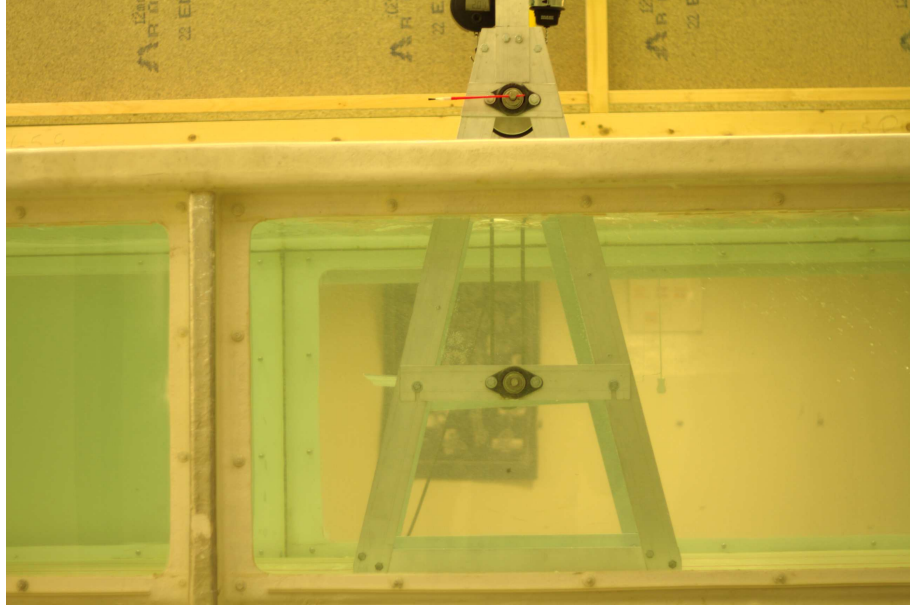
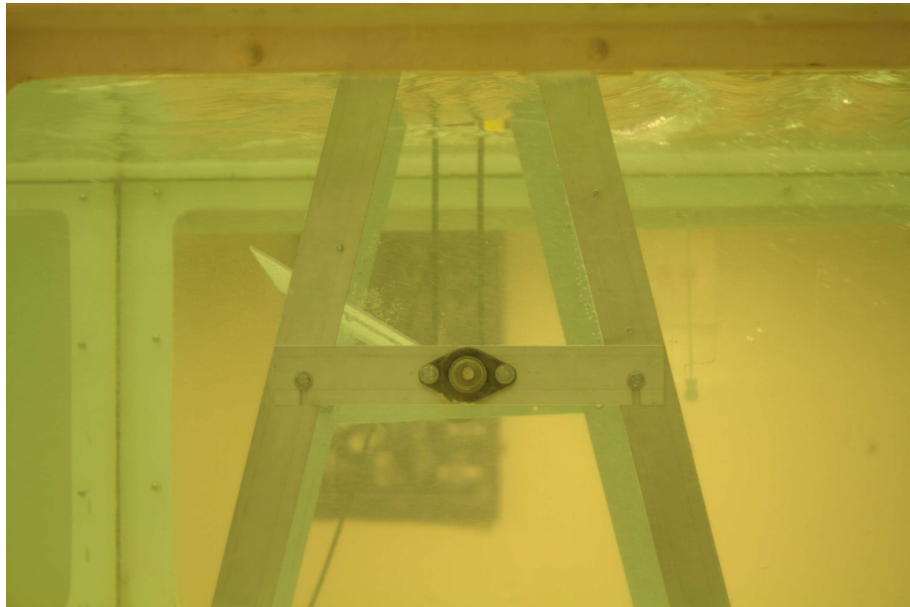*Figure 4.9: The measurement equipment when in the tank.*

Figure 4.10: The blade in fixed position in the tank.

red intensity, would show a red pencil on black background. This image was then turned into a binary image (i.e. black and white), with the white color representing the pencil. Those binary images can be seen in figure 4.12 When this was done the centroid area of the white portion of the image was found, resulting in a certain pixel value in the middle of the white area. And by knowing the center point of
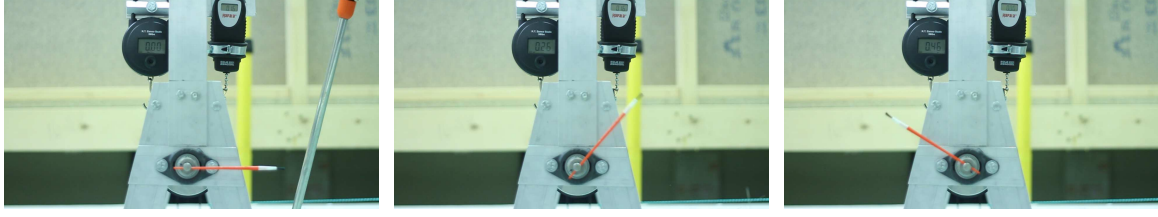
Figure 4.11: Original images as captured on video camera

Figure 4.12: Processed images ready for angle calculation

rotation the angle was found with

$$\theta = arctan\left(\frac{y}{x}\right) \tag{4.1}$$

Using these steps to measure the angle of the blade could be used either for a blade in fixed position or for a blade that is rotating. In the latter case, angle as a function of time could be plotted as can be seen in fig. 4.13 and the angular velocity could be determined.
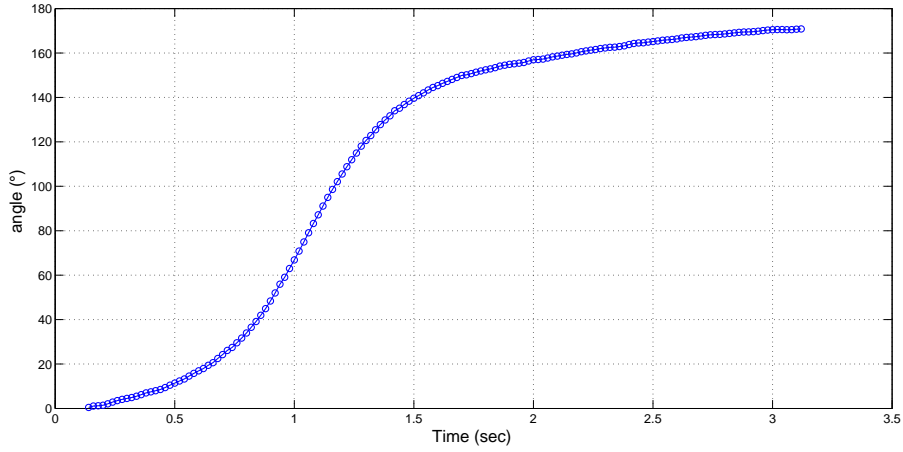

Figure 4.13: Plate angle as a function of time.

5. Results

Results for choosing the right mesh, validation of the numerical model and finding the optimum angular velocity are summarized here.

5.1. Mesh independency

It is important that the quality of the chosen mesh is good enough so that the solution of the problem is independent of it. Three different meshes were constructed, each with different amount of cells. The refinement of the mesh was mainly done around the plate itself, so the outer region for each mesh is in principle the same. Table 5.1 shows the amount of cells for each mesh and the reduction of cells for the medium and coarse mesh as relative to the fine mesh. The fine mesh was chosen as the reference mesh since increasing the amount of cells further for this 2D problem leads to impractical CPU time for flow calculations.

Table 5.1: Mesh parameters.

Mesh	Number of cells	Cell reduction
Fine	133427	-
Medium	92728	30.5%
Coarse	33904	74.6%

5.1.1. Torque comparison

The torque acting on the blade is the most important parameter in this study. Therefore it is logical to compare the quality of different meshes by comparing the average torque acting on the blade for each mesh. The torque curve over the whole 180° rotation was plotted and the average torque was calculated. Figure 5.1 shows the torque curve for each mesh. The average torque can be seen in table 5.2 for each mesh.
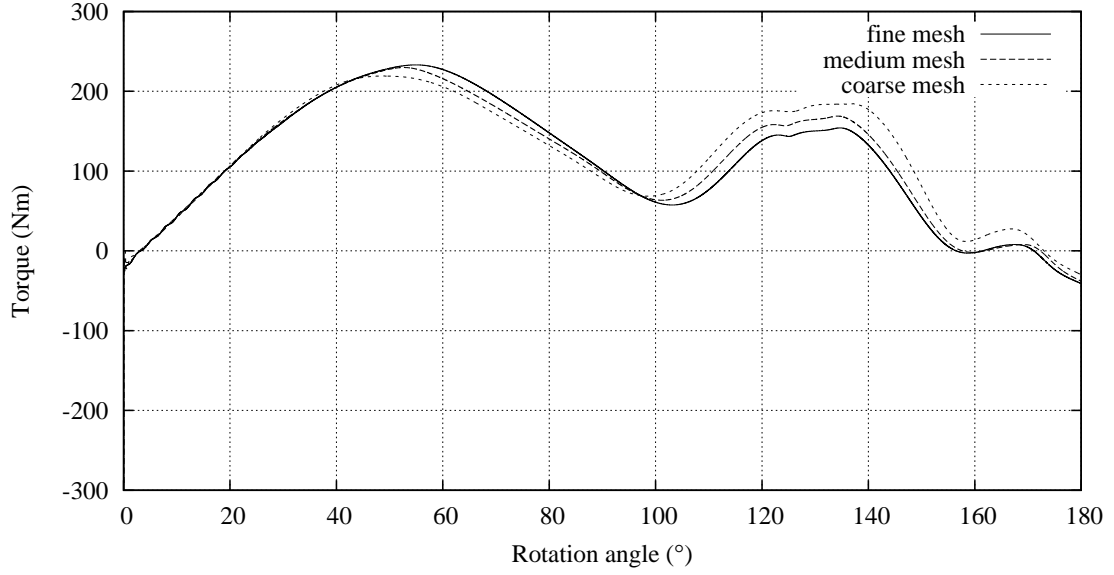
5. Results

Figure 5.1: Torque as function of rotation angle for each mesh.

For a 2D model it can be assumed that the error reduction is proportial to N where N represents the number of cells. If a prediction of the exact solution exists then average torque difference for each mesh against the exact solution can be obtained. Then by plotting the logarithm of this difference versus the logarithm of the cell number and fitting a best line through that data, gives a certain slope. This slope should be equal to unity when the prediction for the exact solution is correct. This was done in this case and the $\log(\overline{T} - T_{prediction})$ vs. $\log(N)$ graph can be seen in fig. 5.2. The value of the predicted exact solution giving slope equal to unity for the fitted line was $T_{predict} = 107.87[Nm]$. The relative error was then calculated using this value

$$\epsilon_{rel} = \frac{\overline{T}_i - \overline{T}_{predict}}{\overline{T}_{predict}} \tag{5.1}$$

where $\overline{T}_{predict}$ is the exact average torque and $\overline{T}_i$ is the average torque for either fine, medium or coarse mesh, depending on which is under study.

Table 5.2: Average torque for each mesh and the discretization error.

Mesh	$\overline{T} [Nm]$	ϵ_{rel}
Fine	110.59	2.53%
Medium	113.25	4.99%
Coarse	119.55	10.83%

This method of estimating the discretization errors is not accurate but it gives an idea of the order of magnitude for the discretization errors.
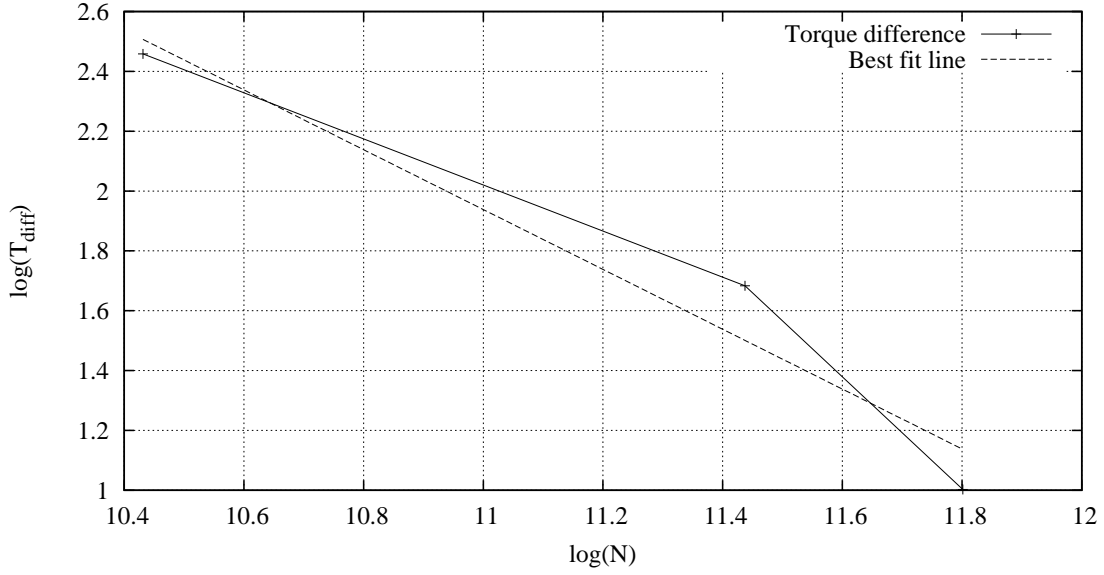
Figure 5.2: Graph used to estimate the magnitude of the discretization errors.

5.1.2. Point comparison

Points where velocity and pressure are measured were located at four different positions in the flow domain to be able to have a different comparison criteria than only the torque acting on the blade. Generally there were not much difference between the meshes for either flow variable. The locations of measurement points in the flow domain can be seen in figure 5.3. The comparison of the measured flow variables for each mesh was plotted for all the points and the plots investigated. Flow variables measured at point 3 behind the plate can be seen in figures 5.4 and 5.5. Figures from other points can be seen in A.1.

5.1.3. Choosing the right mesh

When choosing the right mesh several factors need to be considered with respect to discretization errors.
The main parameter under study here is the average torque acting on the blade and it is important that the discretization errors are not influencing it substantially. The numerical model is not intented to be a detailed simulation of the physical model. The behaviour of the numerical model is the most important factor and if it behaves similar to the physical model, it is acceptable. The CPU time was long for the fine mesh, too long to be practical for the timeframe of this study. The point measurements do not show any behaviour that was not suspected (e.g. figure 5.4 and figure 5.5).
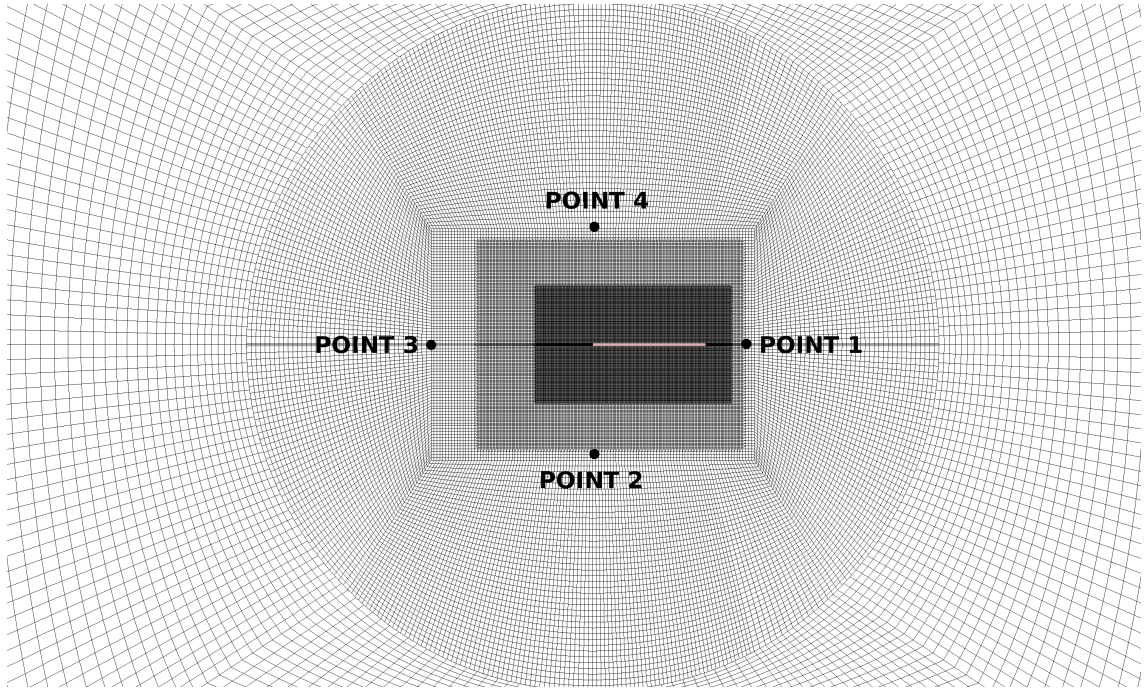When taking everything together, the medium quality mesh was chosen to be the
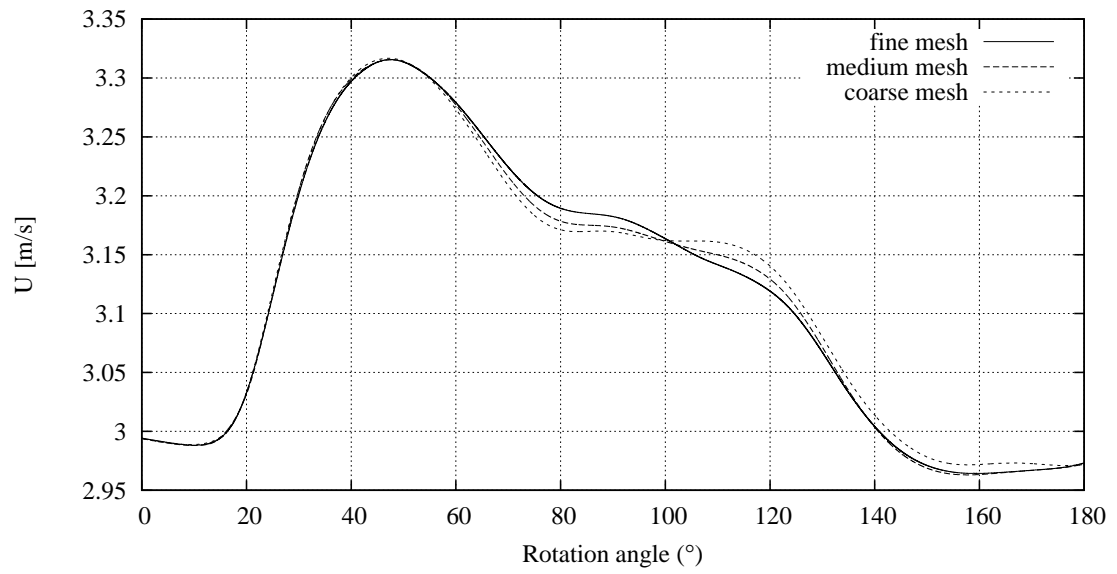
Figure 5.3: Point locations.

Figure 5.4: Velocity for each mesh at point 3.

mesh to be used in this study since it provides reasonable accuracy and CPU time is not a limiting factor.
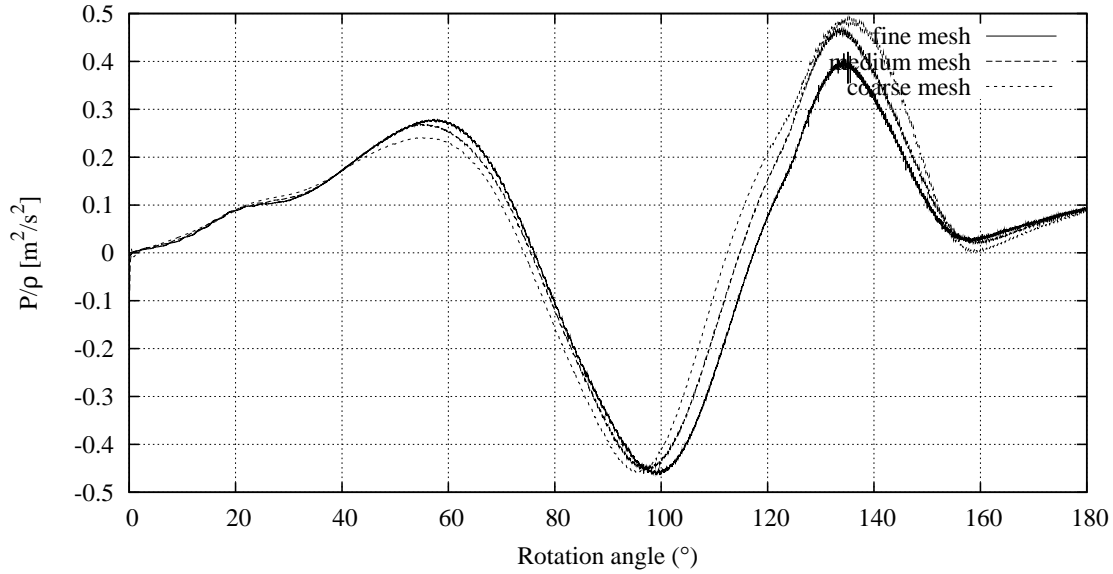
Figure 5.5: Pressure for each mesh at point 3.

5.2. Validating the numerical model

It is important to validate numerical models of fluid flow problems with experimental data so that the physical behaviour of the model can be trusted to show similarity with the real physical behaviour.

As described before, the model was validated with the data gathered from the process described in section 4.2. There were fluctuations in the torque measured for each angle and an average of these values was taken to be the representative value for that specific angle.

In the simulations the blade rotated at 50rpm until it reached a certain angle and then it was stopped. This was done for five different angles, the same angles that were used in the measurements. Table 5.3 shows the measured and simulated values of the torque for each of the five angles and their difference in percentages. It also shows the theoretical value for the blade at 90° that was found by using the drag coefficient for a 2D blade as given in (Crowe et al., 2005). The torque in that case was calculated as follows

$$T = rF = r\,C_d\frac{1}{2}\rho v^2 A \tag{5.2}$$

where T is the torque, r is equal to half of the blade length, $C_d = 2.0$ is the drag coefficient (2D blade), ρ is the fluid density, v is the fluid velocity and A is the surface area of the blade.

There is a difference between the measured and simulated values. The flowmeter in the water tank did not show constant flow velocity with fluctuations up to ±0.04 m/s, affecting the measured torque. The available energy in the flow is related to its velocity in the power of three, twofold increase in velocity leads to eight times increase in available power. Other factors such as free-surface effects and

Table 5.3: *The measured and simulated torque for five different angles.*

	25°	60°	90°	129°	152°
Measured [Nm]	2.78	3.34	4.02	3.53	2.25
Simulated [Nm]	3.17	4.04	5.10	5.22	3.73
Difference [%]	11.51	20.96	26.87	47.88	65.78
Theoretical [Nm]	-	-	3.00	-	-

non-constant velocity profile over the surface area of the channel due to bottom boundary layer effects were not included in the numerical model. Estimation of the scale of influence of these factors are not done in this study.

From table 5.3 it can be seen that the simulated value for 129° angle is higher than for the 90° angle. This can be explained by the irregular structure of the vortex shedding behind the plate for the 129° angle. A steady-state value was not reached since the Reynolds number is $Re = 0.4 \cdot 0.25/10^6 = 10^5$, resulting in unsteady vortex shedding. A value of the torque was needed and eq. 3.27 was used to calculate it. Figures 5.6 and 5.7 show the fluctuation of the torque for either angle when the blade has stopped and the effect of the blade stopping has dissipated. If a longer simulation had been conducted, a more accurate average value of the torque for the higher angle would be reached. The vortex shedding for the 90° angle is more regular and the average value there is more accurate.
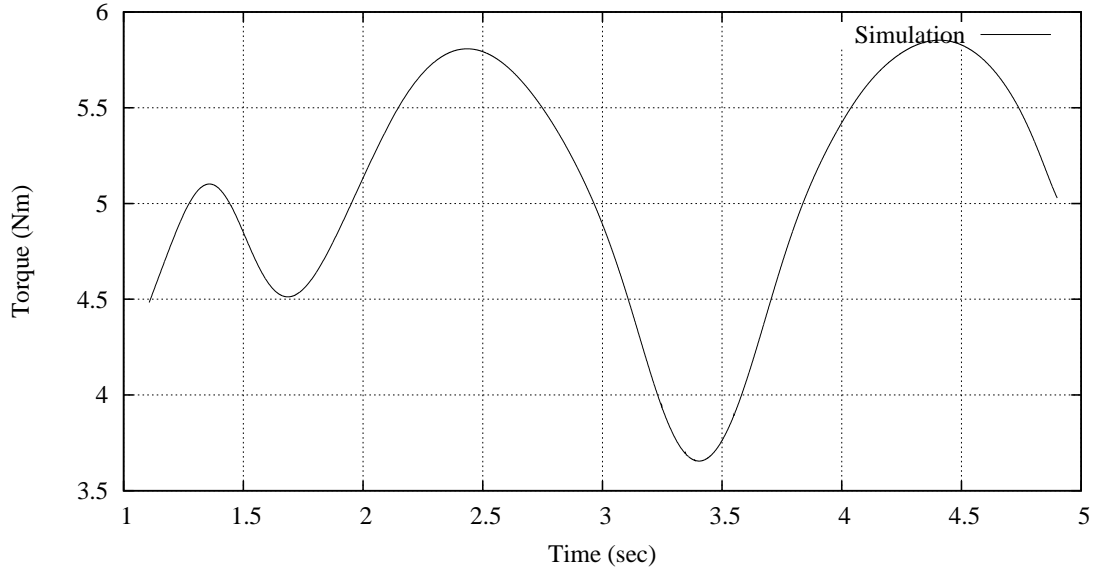

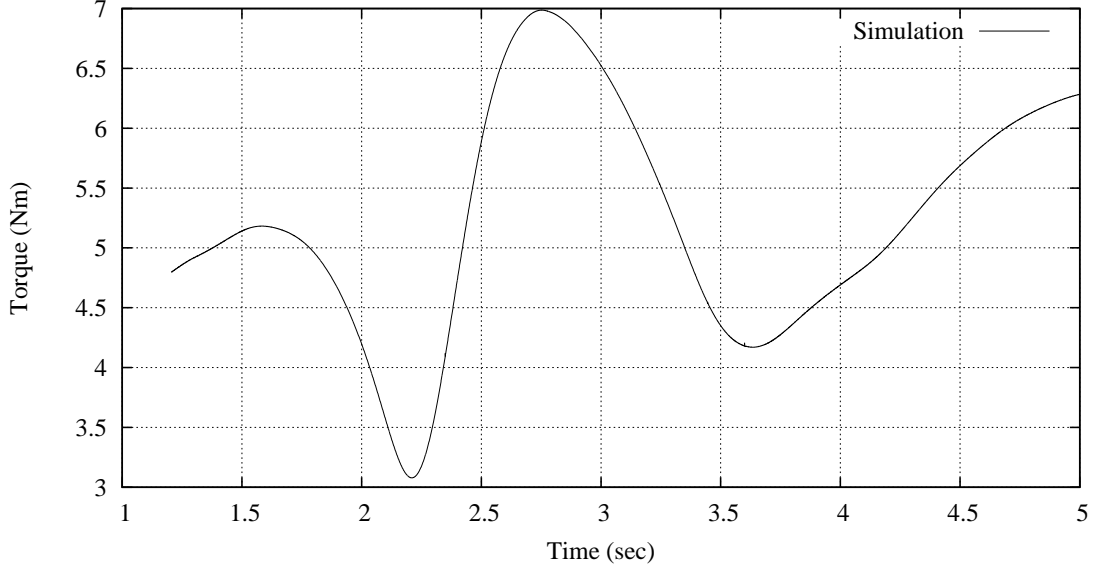Figure 5.6: *The torque fluctuation for a 90° angle.*

Figure 5.7: The torque fluctuation for a 129° angle.

5.3. Finding the optimum angular velocity

Dimensional analysis of this problem, assuming that viscosity is not important because of high Reynolds number, shows that there is a relation between the following dimensionless parameters. This relation is given as

$$\frac{T\omega}{\rho V^3 D^2} = g\left(\frac{\omega D}{V}, \frac{L}{D}\right) \tag{5.3}$$

where T is the torque, ω is the angular velocity, V is the free-stream velocity, D is the length of the blade, L is the width of the blade (i.e. length in the z-direction) and ρ is the density of the fluid. The term on the left can be defined as a dimensionless power coefficient, the first term on the right as a dimensionless velocity and the second term on the right is the aspect ratio of the blade.

Table 5.4: The parameters for the three different cases.

Case	length (m)	fluid vel. (m/s)	*Re*
1	0.25	2.5	6.25×10^5
2	3.00	2.5	7.50×10^6
3	0.25	0.4	1.00×10^5

Assuming that the aspect ratio of the blade is constant it is possible to find the optimum dimensionless velocity that maximizes the power output. This was done here for three different cases, to identify if they have the same optimum dimensionless velocity. The first case was the experimental blade with fluid velocity of 2.5 m/s, next case was with a larger plate with the same fluid velocity and the last case was

5. Results

with the experimental blade but now with fluid velocity of 0.4 m/s. The larger plate is a 12 times scaled up version of the smaller plate. Table 5.4 shows the relevant parameters for the three different cases. Figure 5.8 shows the two curves relating the dimensionless parameters for each case.
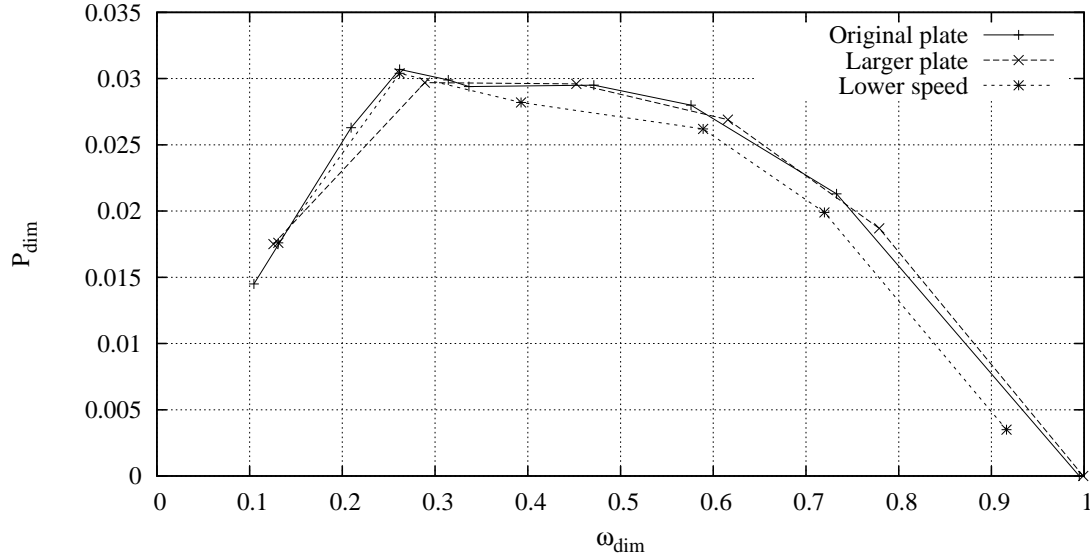

Figure 5.8: The curves showing the relation between the dimensionless parameters.

where P_{dim} and ω_{dim} are defined as

$$P_{dim} = \frac{T\omega}{\rho V^3 D^2} \qquad \omega_{dim} = \frac{\omega D}{V} \tag{5.4}$$

Figure 5.8 shows that assuming Reynolds number independency is correct since the curves for each case are similar and same relation can be seen for all of them. More data points would reveal better curves, especially around the maximum point. The optimal point is in the range $0.3 \leq \omega_{dim} \leq 0.5$. The optimum angular velocity for either blade size can easily be determined by rearranging eq. 5.4, as shown below

$$\omega = \frac{\omega_{dim} V}{D} \tag{5.5}$$

36

6. Discussion and conclusion

A numerical model of a rotating flat plate was developed and validated with experimental data. The model was built using OpenFOAM and a dynamic mesh to account for the rotation. Although for its high learning curve, OpenFOAM is ideal for simulations using a dynamic mesh since specific tools have been developed for that type of simulations. Changes to one of OpenFOAM's classes was done to be able to simulate time dependent blade rotation. That is important for further development of the numerical model. This was also done so the measurements could be simulated in enough detail.

The original measurement setup was altered since the equipment available was not able to capture the measured variables in the way they were supposed to. First the plan was to let the blade rotate 180° and measure the torque acting on it but the response time of the digital scales that measured the torque was not good enough to give accurate data. The alteration was to fix the blade in certain positions and measure the torque. When validating the numerical model, the blade in the simulation rotated into these certain positions and was then stopped. Then the average torque was calculated after the effect of stopping the blade had dissipated. This setup was the best option for the timeframe available for this project.

The numerical model gives different values than were measured, but the order of magnitude is the same for both values. The main uncertainty is the flow velocity in the water tank, where fluctuations were noticed. The model does not include free-surface effects nor the non-linear velocity profile because of boundary layer influence due to the bottom of the water tank. The simulated values were found to be on average 34.6% higher than the measured values. A longer simulation time would give a better estimate of the average values of the torque since the vortex shedding structure is quite irregular and a larger time interval (i.e. more samples) leads to more accuracy.

By using dimensional analysis, a relation between a dimensionless power coefficient P_{dim} and dimensionless velocity ω_{dim} was found. An optimum dimensionless velocity was found to be the same for different cases, lying in the range of $0.3 \leq \omega_{dim} \leq 0.5$. This result confirms, that assuming that the flow in this problem is independent of the Reynolds number, is correct. The shearing force is less than 1% of the pressure force acting on the blade.

6. Discussion and conclusion

The numerical model has its limitations. Cavitation (i.e. phase change) is not included in it and it is interesting to investigate what is the maximum limit of flow velocity before cavitation occurs. Although the phase change is not included the pressure calculation in the simulations can be used to determine if the pressure drop is enough to initiate cavitation (see appendix A.2). The free-surface effects are not modelled but since the device developed by Valorka is considered to work below $10m$ depth it is questionable how much they affect the flow. Finally when the device is connected to the electrical grid it would have a large rotational inertia, resulting in almost constant angular velocity. But in principle this problem is a Solid-Fluid-Interaction (SFI) problem and if a force big enough is acting on the device it will affect the angular velocity.

Further development of the numerical model is planned. For future work a blade optimization and developing a 3D model could be done using the model built in this study. The blade optimization would give an idea what blade shape is the most preferable for capturing the kinetic energy of the ocean currents. Changing the blade shape is done rather easily in OpenFOAM. When the mesh is created, a text file with all the mesh points is written out. The points in this file can be taken and manipulated by defining a function that rearranges these points so the shape of blade changes in the way that the function prescribes.This option is achievable in the near future. Developing a 3D model is a more comprehensive task than the blade optimization. By using the GGI, the stator-rotor interface could have a spherical shape. In that way the rotating part would become a sphere that could rotate around two axis, like the real physical model. The turbine rotating about the main shaft and the blades rotating around their shafts. This option should be considered as a long term goal.

Bibliography

ARC (2011). Technology description and development status. [Online] Available from: <http://www.atlantisresourcescorporation.com/marine-power/atlantis-technologies.html> [Accessed: 20th. April 2011].

Audi, E. (2009). Comparison of pressure-velocity coupling schemes for 2d flow problems. In *International Conference on Advances in Computational Tools for Engineering Applications (ACTEA)*, pages 245–248.

BBC (2011). News feed on Pulse Generation newest project. [Online] Available from: <http://www.bbc.co.uk/news/10153669> [Accessed: 20th. April 2011].

Beaudoin, M. and Jasak, H. (2008). Development of a generalized grid interface for turbomachinery simulations with openfoam. In *Open Source CFD International Conference*, Berlin, Germany.

Bedard, R., Jacobson, P. T., and Previsic, M. (2010). An overview of ocean renewable energy technologies. *Oceanography*, 23(2):22–31.

Boehlert, G. W. and Gill, A. B. (2010). Environmental and ecological effects of ocean renewable energy development. *Oceanography*, 23(2):68–81.

Boyle, G. (2004). *Renewable Energy: Power For a Sustainable Future*. Oxford University Press, New York, USA, 2nd. edition.

Brundtland et al. (1987). Report of the world commission on environment and development: Our common future. [Online] Available from: <http://www.un-documents.net/wced-ocf.htm> [Accessed: 2nd. May 2011].

Crowe, C. T., Elger, D. F., and Roberson, J. A. (2005). *Engineering Fluid Mechanics*. John Wiley Sons, Inc., New Jersey, USA, 8th. edition.

Davidson, L. (2011). *An Introduction to Turbulence Models*. Department of Fluid and Thermo Dynamics, Chalmers, Göteborg, Sweden, 2nd. edition.

DECC (2011). News feed about Tidal Energy Ltd. project status. [Online] Available from: <http://www.decc.gov.uk/en/content/cms/news/pn11_034/pn11_034.aspx> [Accessed: 20th. April 2011].

BIBLIOGRAPHY

EIA (2011). *Annual Energy Outlook 2011 with Projections to 2035.* U.S. Energy Information Administration, Washington DC, USA.

European Union (2010). Europe's energy portal. [Online] Available from: `<http://www.energy.eu/#renewable>` [Accessed: 2nd. May 2011].

Ferziger, J. and Peric, M. (2002). *Computational Methods for Fluid Dynamics.* Springer-Verlag, Berlin, Germany, 3rd. edition.

Hammerfest Strom AS (2011). Technology description and development status. [Online] Available from: `<http://www.hammerfeststrom.com/products/tidal-turbines/>` [Accessed: 20th. April 2011].

Lunar Energy Ltd. (2011). Technology description and development status. [Online] Available from: `<http://www.lunarenergy.co.uk/productOverview.htm>` [Accessed: 20th. April 2011].

MCT (2011). Technology description and development status. [Online] Available from: `<http://www.marineturbines.com/21/technology/>` [Accessed: 20th. April 2011].

Ocean Flow Energy Ltd. (2011). Development status. [Online] Available from: `<http://www.oceanflowenergy.com/development-status.html>` [Accessed: 20th. April 2011].

OpenHydro (2011). Technology description and development status. [Online] Available from: `<http://www.openhydro.com/development.html>` [Accessed: 20th. April 2011].

Otic, I. and Cheng, X. (2010). Piso-simple-type algorithms for transient incompressible turbulent flows. In *Annual Meeting 2010*, volume 102, page 634. Transactions of the American Nuclear Society.

Pulse Generation Ltd. (2011). Technology description and development status. [Online] Available from: `<http://www.pulsetidal.com/40.html>` [Accessed: 20th. April 2011].

Riemslagh, K., Vierendeels, J., and Dick, E. (1998). Two-dimensional incompressible navier-stokes calculations in complex-shaped moving domains. *Journal of Engineering Mathematics*, 34:57–73.

Robinson, E. and Byrne, G. (2008). Methodology for modeling tidal turbine characteristics. In *OCEANS 2008*, Quebec City, Canada. IEEE. doi:10.1109/OCEANS.2008.5151948.

Rourke, F. O., Boyle, F., and Reynolds, A. (2010). Tidal energy update 2009. *Applied Energy*, 87:398–409.

Rutherford, A. (1989). *Vectors, Tensors and the Basic Equations of Fluid Mechanics.* Dover Publications Inc., New York, USA.

Sutherland, I. and Hodgman, G. (1974). Reentrant polygon clipping. *Communications of the ACM*, 17:32–42.

Tennekes, H. and Lumley, J. (1974). *A First Course in Turbulence.* MIT Press, Massachusetts, USA, 3rd. edition.

Tidal Energy Ltd. (2011). Technology description. [Online] Available from: `<http://www.tidalenergyltd.com/technology.htm>` [Accessed: 20th. April 2011].

Turner, N. and Owen, A. (2007). The development of a tidal turbine for deployment in areas with slow moving tidal flows. In *OCEANS 2007 - Europe*. IEEE. doi:10.1109/OCEANSE.2007.4302428.

Valorka (2011). Overview of the company's history and current development. [Online] Available from: `<http://www.valorka.is>` [Accessed: 10th. May 2011].

Valorka.ehf (2010). Report on testing of the valorka turbine. Technical report, RANNIS Technology Development Fund.

Verdant Power Inc. (2011). Technology description and development status. [Online] Available from: `<http://verdantpower.com/what-initiative/>` [Accessed: 20th. April 2011].

WEC (2010). *2010 Survey of Energy Resources.* World Energy Council, London, UK, 22nd. edition.

WIKKI (2011). Consultancy and software development in computational continuum mechanics. [Online] Available from: `<http://www.wikki.co.uk/>` [Accessed: 2nd. May 2011].

A. Appendix

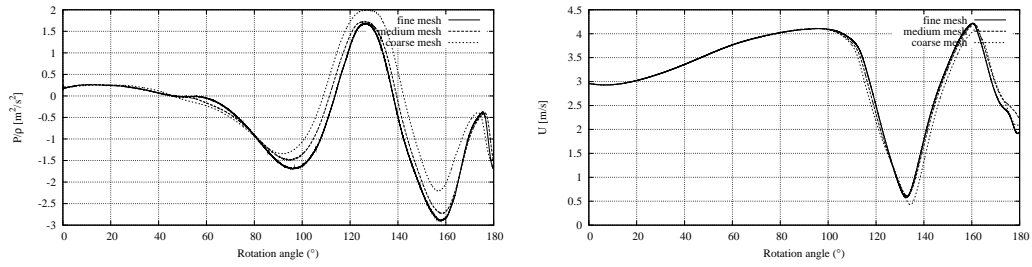## A.1. Point comparison figures

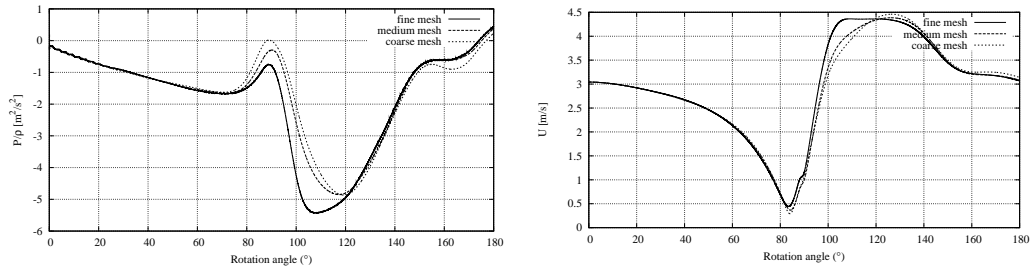*Figure A.1: The flow variables at point 1.*

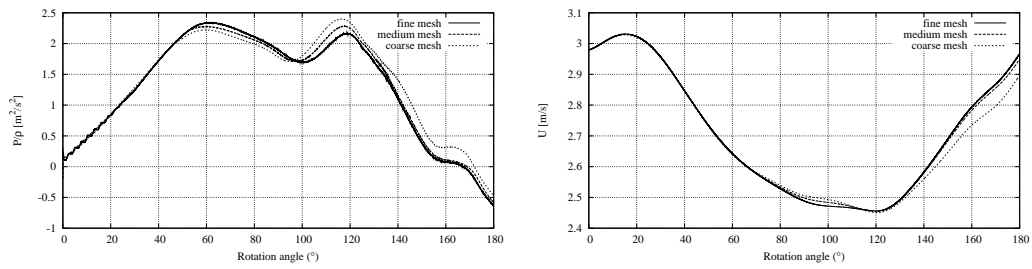*Figure A.2: The flow variables at point 2.*

Figure A.3: The flow variables at point 4.

A.2. Highest pressure and velocity values in the flow domain

The pressure and velocity are calculated in the simulations and below are images showing their values throughout the solution domain. The pressure calculation can be used to see if cavitation occurs within the system. The images shown here are from the first case in section 5.3. The highest and lowest values of pressure and velocity for the whole case can be seen on the scale on the right side of the images.
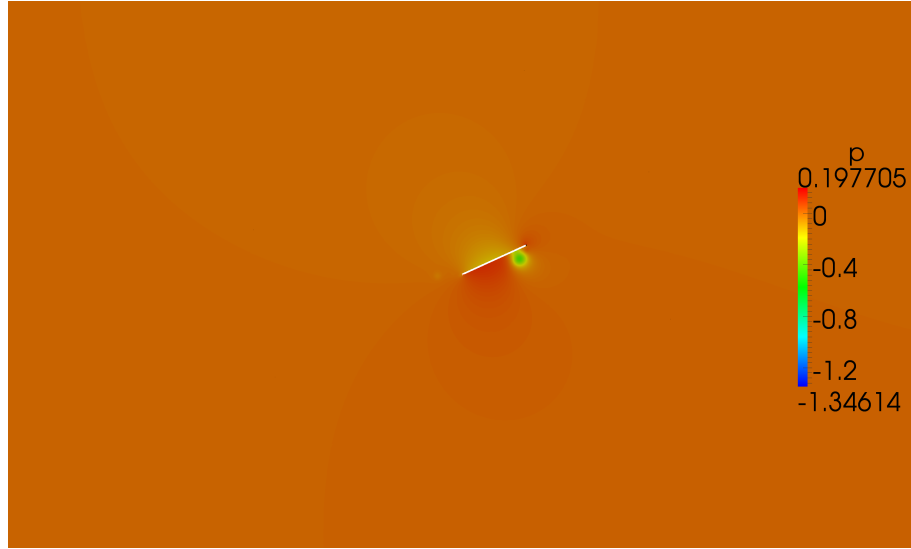

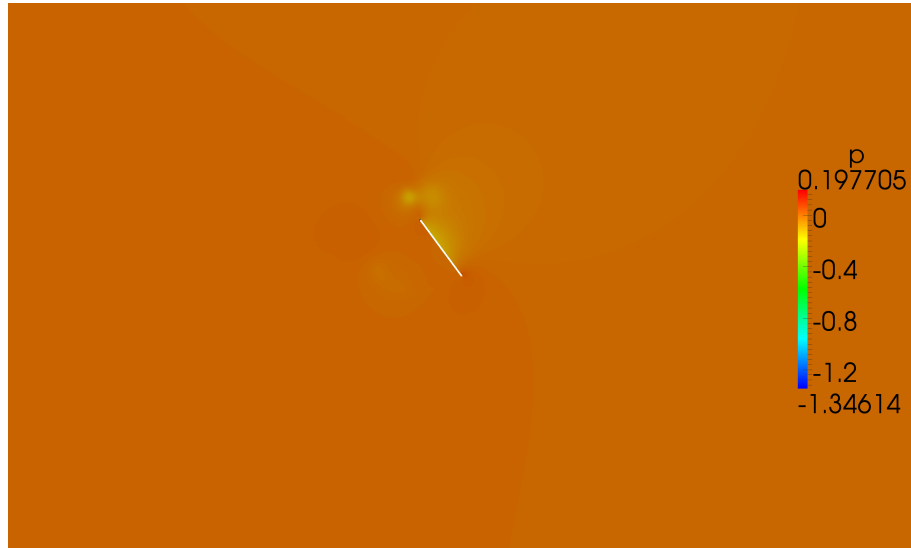*Figure A.4: Pressure distribution in the beginning of the simulation.*

Figure A.5: Pressure distribution later in the simulation.
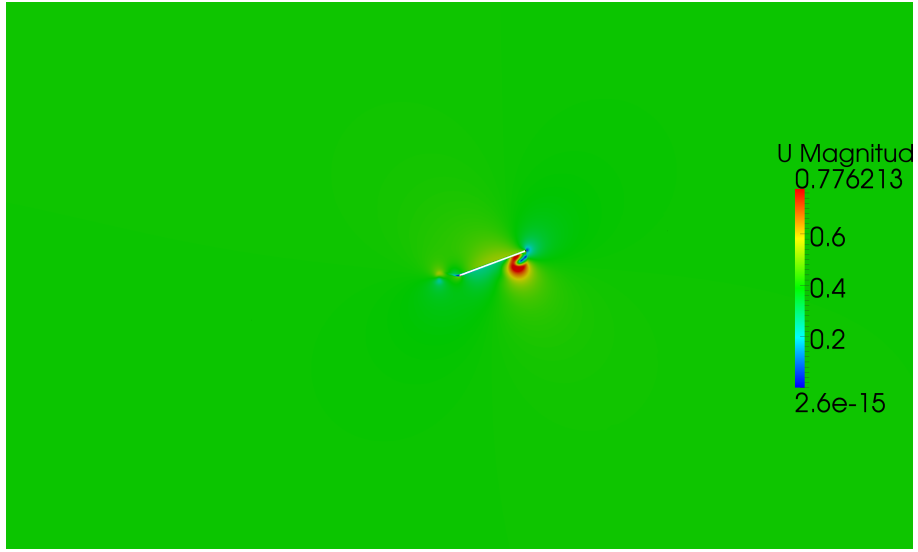
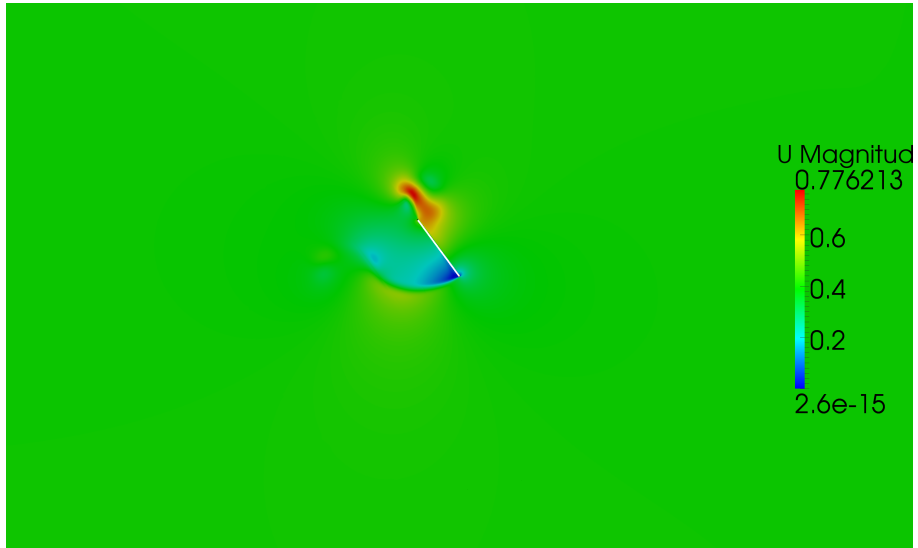*Figure A.6: Velocity distribution in the beginning of the simulation.*

Figure A.7: Velocity distribution later in the simulation.